

NANO EXPRESS

Open Access



Effect of Synthesis Temperature on Structure and Magnetic Properties of $(\text{La,Nd})_{0.7}\text{Sr}_{0.3}\text{MnO}_3$ Nanoparticles

Yulia Shlapa^{1*}, Sergii Solopan¹, Andrii Bodnaruk², Mykola Kulyk², Viktor Kalita², Yulia Tykhonenko-Polishchuk³, Alexandr Tovstolytkin³ and Anatolii Belous¹

Abstract

Two sets of Nd-doped $\text{La}_{0.7}\text{Sr}_{0.3}\text{MnO}_3$ nanoparticles were synthesized via sol-gel method with further heat treatment at 1073 and 1573 K, respectively. Crystallographic and magnetic properties of obtained nanoparticles were studied, and the effect of synthesis conditions on these properties was investigated. According to X-ray data, all particles crystallized in the distorted perovskite structure. Magnetic parameters, such as saturation magnetization, coercivity, Curie temperature, and specific loss power, which is released on the exposure of an ensemble of nanoparticles to AC magnetic field, were determined for both sets of samples. The correlation between the values of Curie temperature and maximal heating temperature under AC magnetic field was found. It was revealed that for the samples synthesized at 1573 K, the dependences of crystallographic and magnetic parameters on Nd content were monotonous, while for the samples synthesized at 1073 K, they were non-monotonous. It was concluded that Nd-doped $\text{La}_{0.7}\text{Sr}_{0.3}\text{MnO}_3$ nanoparticles are promising materials for self-controlled magnetic hyperthermia applications, but the researchers should be aware of the unusual behavior of the particles synthesized at relatively low temperatures.

Keywords: Manganite nanoparticles: magnetic hyperthermia, Distorted perovskite structure, Oxygen non-stoichiometry, Magnetization, Curie point, Coercivity, Specific loss power (SLP)

PACS: 61.46.Df, 75.75.Cd, 81.07. Bc

Background

Nanoparticles of ferro- and ferrimagnetic materials have been of particular scientific and practical interest due to their possibility to be applied in medicine [1–4]. The most promising fields of medical applications are targeted drug and bioactive object delivery [5, 6], cellular monitoring of bioactive systems (for example, magnetic resonance imaging (MRI)) [7], magnetic hyperthermia [8, 9], etc. The close relation between modern development of cellular and tissue technology and the latest developments in biochemistry, biophysics, and nanotechnology has been at the heart of such interest [10, 11].

At present, researchers consider spinel nanoferrites (for instance, magnetite Fe_3O_4) as principal candidates for various applications in biomedicine. Iron oxide nanoparticles have already been used as the contrast agents in MRI. They significantly enhance MRI signal and cause minimal side effects on living organisms [12]. At the same time, new materials are examined with the aim to improve efficiency and widen the areas of applications. In vivo studies [13] show that MnFe_2O_4 nanoparticles display much better characteristics than Fe_3O_4 ones, while using them as contrast agents for MRI. The advantage of Tb-doped Fe_3O_4 nanoparticles consists not only in enhanced magnetic characteristics but also in the possibility to investigate the fluorescent properties [14]. It should be mentioned that all these materials did not demonstrate any cytotoxicity during cytological studies [15].

* Correspondence: yuliashlapa@ukr.net

¹V.I. Vernadskii Institute of General and Inorganic Chemistry of the NAS of Ukraine, 32/34 Palladina Ave., Kyiv 03142, Ukraine

Full list of author information is available at the end of the article

A great deal of work has been aimed at a search for new materials for magnetic hyperthermia applications [9, 10, 16]. To be successfully used in hyperthermia therapy, magnetic nanoparticles have to meet some important requirements, such as to be biocompatible, weakly agglomerated (with the aim to prevent the clots formation), and characterized by the absence of residual magnetization. In addition, they have to heat up effectively under the action of an AC magnetic field [16]. However, the heating of tumor tissue without damaging the surrounding structures has been a challenge to scientists. In the presence of an AC magnetic field, the heat produced by the particles cannot be controlled, as these particles retain their magnetic properties even at sufficiently high temperatures. The temperature at which they change their magnetic behavior from ferro- or ferromagnetic to paramagnetic is called Curie temperature (T_C). Thus, T_C point near 50 °C can be used as in vivo switch, since in the presence of AC magnetic field, the temperature will not rise above it, and further heating will stop [17].

The nanoparticles of spinel ferrites display relatively high values of T_C (for instance, T_C of Fe_3O_4 is 585 °C) [18]. At the same time, the materials like $\text{La}_{1-y}\text{Sr}_y\text{MnO}_3$ look very promising for the hyperthermia applications, since they have relatively large magnetic moment at room temperature and their phase-transition temperature can be easily tuned in the range of 0–90 °C by changing the chemical composition [19].

Lanthanum-strontium manganites $\text{La}_{1-y}\text{Sr}_y\text{MnO}_3$ crystallize in the distorted perovskite structure and display ferromagnetic properties over the wide range of Sr-content ($0.15 \leq y \leq 0.60$) [20, 21]. Their Curie temperature strongly depends on the chemical composition: it demonstrates the maximal value at $y \approx 0.3$ ($T_{C_{\text{max}}} \approx 370$ K) and quite sharply decreases as y deviates from 0.3. Earlier, it was shown that fine controlling of the Curie point within the narrow temperature range can be reached by low-level substitutions in manganese sublattice [22]. At the same time, partial substitutions of La^{3+} ions by other rare-earth ions (for instance, by Nd^{3+}) may be one more possible way of fine-tuning the phase-transition temperature, since magnetic interactions in manganites are sensitive to the lattice parameters and strength of local lattice distortions [23]. Since the ionic radii of La^{3+} (1.36 Å) and Nd^{3+} (1.27 Å) ions are quite close, the Curie temperature is expected to be changed more softly upon substitutions of such kind.

Unfortunately, the properties of substituted manganites are very sensitive to the synthesis conditions. As shown in [21, 24–27], the changes of heating temperature or annealing duration may lead to the deviation of an oxygen content from stoichiometric value.

According to [21], the stoichiometry of substituted manganites and oxidation state of Mn ions depend not only on Sr-content but also on atmosphere, temperature, and duration of heat treatment. Moreover, the results reported in [24, 26] indicate that the synthesis under the same conditions does not guarantee the same degree of oxygen non-stoichiometry in the samples with different chemical composition. The authors of [24] came to a conclusion that these effects are likely to originate from close interdependence between crystallographic parameters and oxygen diffusion coefficient: the contraction of crystal lattice makes oxygen diffusion more difficult, and this eventually results in the dependence of the degree of oxygen non-stoichiometry on such factors as structure, chemical composition, and others.

Up to now, the most of studies have been dealing with the substituted manganites obtained at relatively high temperatures (≥ 1300 K) [28, 29]. Recently, the investigation of manganite nanoparticles and their properties has become more relevant [30]. In most cases, lower temperatures are used in the process of the synthesis of nanoparticles (around 1000 K and lower) [31, 32]. Previous data show that in the latter case, the dependence of oxygen non-stoichiometry on the chemical composition can be quite significant (even for the synthesis of a series of samples under the same conditions) [21]. However, there are no any more detailed investigations of this issue.

The aim of this study is synthesis of $\text{La}_{0.7-x}\text{Nd}_x\text{Sr}_{0.3}\text{MnO}_3$ ($x = 0-0.1$) nanoparticles via sol-gel method with further annealing at different temperatures, investigation of their structural and magnetic properties, and clarifying the effect of the chemical composition and synthesis conditions on the crystallographic and magnetic parameters.

Methods

Nd-doped ($\leq 10\%$) manganite nanoparticles were synthesized via sol-gel method. The aqueous solutions of metal salts $\text{La}(\text{NO}_3)_3$, $\text{Nd}(\text{NO}_3)_3$, $\text{Sr}(\text{NO}_3)_3$, and $\text{Mn}(\text{NO}_3)_2$ were used as the starting reagents. Necessary amounts of starting solutions were mixed, citric acid and ethylene glycol were added as the gel forming agents. The obtained reaction mixture was heated with stirring at 353 K. The polymer gel was formed during polyesterification reaction, which took place at pH = 9. An amorphous precursor $(\text{La},\text{Nd},\text{Sr})\text{MnO}_3$, obtained after gel pyrolysis, was subjected to further high-temperature treatment for 2 h: one set at 1073 K, while another set at 1573 K.

X-ray diffraction study (XRD) of the obtained powders was performed using DRON-4 diffractometer ($\text{CuK}\alpha$ radiation). Crystallographic lattice parameters of the

single-phased product were calculated by Rietveld method using FULL-PROF software package. The crystallite size was estimated from XRD line broadening using Scherrer equation:

$$D_{\text{XRD}} = \frac{K \cdot \lambda}{B \cdot \cos \theta} \quad (1)$$

where λ is a wave length, B is the peak width, θ is the Bragg angle, and $K \approx 0.89$ is the shape factor [33].

Magnetic measurements were performed using a LDJ-9500 vibrating sample magnetometer. To analyze the field and temperature dependences of magnetization, hysteresis loops were measured for $-5 \text{ kOe} \leq H \leq 5 \text{ kOe}$ in the temperature range from 110 to 370 K.

For the calorimetric determination of specific loss power (SLP) which is released on the exposure of an ensemble of the particles to AC magnetic field, the ferrofluids based on synthesized magnetic nanoparticles (50 mg/mL) were prepared using 0.1% aqueous agarose solutions. To obtain the fluid temperature T_{fluid} vs residence time τ dependences, the magnetic fluids were placed into the coil, which generated AC magnetic field with a frequency of 300 kHz and amplitude up to 9.5 kA/m. All measurements and calculations were done according to the procedure described in [34]. Specific loss power values were calculated by the formula:

$$\text{SLP} = \frac{C_{\text{fluid}} \times V_s}{m_{\text{powder}}} \times \frac{dT_{\text{fluid}}}{d\tau} \quad (2)$$

where $dT_{\text{fluid}}/d\tau$ is an initial slope of the temperature vs time dependence, C_{fluid} and V_s are the volumetric specific heat and the sample volume, respectively, and m_{powder} is the mass of the magnetic material in the fluid.

Results and Discussion

According to XRD data, the synthesized $\text{La}_{0.7-x}\text{Nd}_x\text{Sr}_{0.3}\text{MnO}_3$ nanoparticles are single-phased and crystallize in the distorted perovskite structure (space group R-3c) even at 1073 K. Representative diffraction patterns for the samples with $x=0.00$ and 0.04 are shown in the insets to Fig. 1. Corresponding structural parameters ($a = b, c, V$) for the nanoparticles, synthesized at 1073 K and 1573 K, were calculated by Rietveld method. The results are summarized in Table 1.

As seen from the data of Table 1, the unit cell volume for $\text{La}_{0.7-x}\text{Nd}_x\text{Sr}_{0.3}\text{MnO}_3$ nanoparticles, synthesized at 1573 K, decreases with growing Nd content. Such behavior points toward isomorphous substitution of larger La^{3+} ions by smaller Nd^{3+} ions. It follows from Fig. 1 that there is a linear change of crystallographic parameters over the range of Nd from 0.0 to

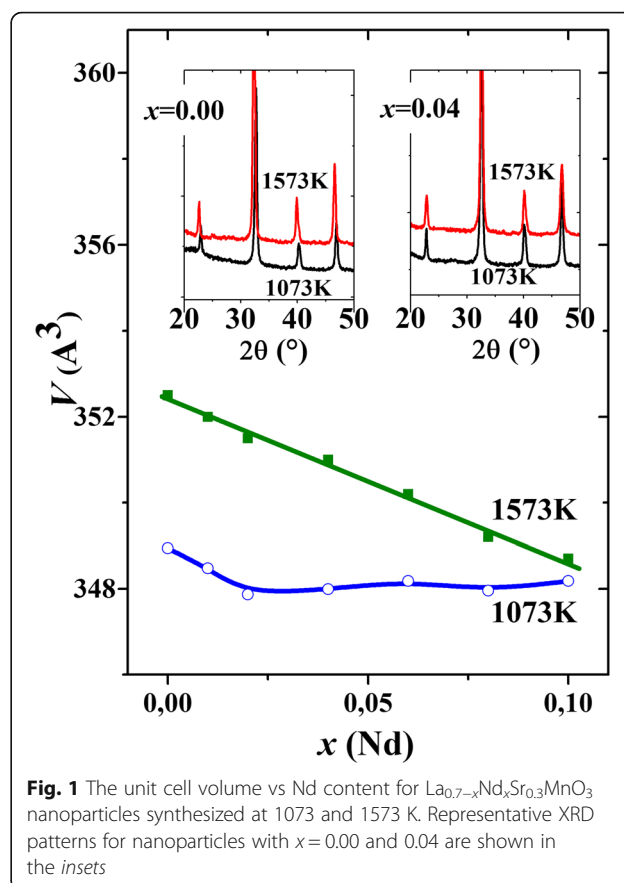


Fig. 1 The unit cell volume vs Nd content for $\text{La}_{0.7-x}\text{Nd}_x\text{Sr}_{0.3}\text{MnO}_3$ nanoparticles synthesized at 1073 and 1573 K. Representative XRD patterns for nanoparticles with $x=0.00$ and 0.04 are shown in the insets

0.1, which means that the system obeys Vegard's law. Thus, a continuous line of solid solutions is formed in this Nd-concentration range. At the same time, the linear $V(x)$ dependence implies that oxygen amount is the same (or quite close) in all samples and it is independent of the Nd concentration.

The non-monotonous relation between crystallographic parameters and Nd-content is observed for $\text{La}_{0.7-x}\text{Nd}_x\text{Sr}_{0.3}\text{MnO}_3$ nanoparticles synthesized at 1073 K (see Fig. 1). This fact can be caused either by incomplete ordering of the crystal structure or by the dependence of oxygen non-stoichiometry on the samples' chemical composition (in this case—on the Nd content). Similar effects, but for the perovskite compounds of other compositions, were reported in [21, 24, 25, 35] and explained by the dependence of oxygen diffusion coefficient on lattice parameters [24] or by stress-induced clustering of oxygen vacancies [25]. It was also shown that Nd-containing manganites usually show a very varied defect structure: depending on composition and heat treatment, vacancies can form on any one or any two of the three sublattices (Ln, Mn or oxygen) [35]. To distinguish between different models of defect formation and mechanisms of stress accommodation in

Table 1 Crystallographic parameters of $\text{La}_{0.7-x}\text{Nd}_x\text{Sr}_{0.3}\text{MnO}_3$ nanoparticles obtained via sol-gel method

x	0.00	0.01	0.02	0.04	0.06	0.08	0.1
$\text{La}_{0.7-x}\text{Nd}_x\text{Sr}_{0.3}\text{MnO}_3$ after 1073 K							
a , Å	5.4911(8)	5.4901(7)	5.4884(4)	5.4867(2)	5.4914(2)	5.4908(2)	5.4933(5)
c , Å	13.3632(1)	13.3498(2)	13.3351(1)	13.3482(7)	13.3326(7)	13.3270(9)	13.3232(1)
V , Å ³	348.94(5)	348.48(9)	347.87(5)	347.99(2)	348.18(2)	347.96(3)	348.18(7)
R_b , %	5.60	9.14	7.06	5.07	4.52	5.87	8.24
R_f , %	8.19	12.8	9.35	6.36	5.77	7.57	11.5
d_{XRD} , nm	31	30	32	37	36	36	39
$\text{La}_{0.7-x}\text{Nd}_x\text{Sr}_{0.3}\text{MnO}_3$ after 1573 K							
a , Å	5.485(1)	5.482(1)	5.479(3)	5.476(2)	5.472(2)	5.466(1)	5.465(2)
c , Å	13.531(5)	13.524(2)	13.520(8)	13.517(6)	13.504(5)	13.498(6)	13.486(1)
V , Å ³	352.5(2)	352.0(1)	351.5(3)	351.0(2)	350.2(2)	349.2(2)	348.7(4)
R_b , %	6.60	7.14	5.80	6.07	5.42	4.92	8.30
R_f , %	8.30	8.80	7.35	6.46	6.77	6.67	5.42

Here, R_b is Bragg factor and R_f is compliance form factor

Nd-containing manganites, a number of additional studies and calculations are necessary, but such activities go beyond the scope of this work.

The crystallite sizes of nanoparticles obtained at 1073 K were calculated from the Sherrer's formula with the use of (110) peak (Table 1). According to the calculations, the crystallite sizes are in the range of 30–39 nm.

Magnetization curves $M(H)$ for $\text{La}_{0.7-x}\text{Nd}_x\text{Sr}_{0.3}\text{MnO}_3$ nanoparticles with $x = 0.00$ and 0.04, synthesized at different temperatures, are shown in the insets to Fig. 2. The measurements were performed at 295 K. Magnetization grows with increasing magnetic field and tends to saturation at $H \geq 1500$ Oe. The general trend is the reduction of saturation magnetization M_s with the increase in Nd content. Also, M_s becomes almost two times lower as synthesis temperature decreases from 1573 to 1073 K.

Figure 2 presents the concentration dependence of the saturation magnetization, $M_s(x)$, for the samples synthesized at 1573 and 1073 K. In the first case, M_s is the monotonous and almost linear function of x . What concerns the second case (synthesis temperature is 1073 K), the saturation magnetization is almost twice lower than M_s for the first series and its values are only weakly dependent on x . The character of the variation of $M_s(x)$ for the samples synthesized at lower temperature is close to that of $V(x)$ dependence (see Fig. 1), which indicates that the peculiar features of both dependences may be of the same nature.

More details of the magnetization behavior can be seen from Fig. 3, where $M(H)$ dependences in the range of the weak magnetic fields are shown. It follows from the $M(H)$ data that the coercivity H_c for the nanoparticles synthesized at lower temperatures (1073 K) are 1.5–2 times higher than H_c for the

nanoparticles synthesized at higher temperature. According to Fig. 3, where the $H_c(x)$ dependences for both series of the samples are shown, the coercivity in both cases is weakly dependent on the Nd content. Strong increase in the coercivity, observed in the first

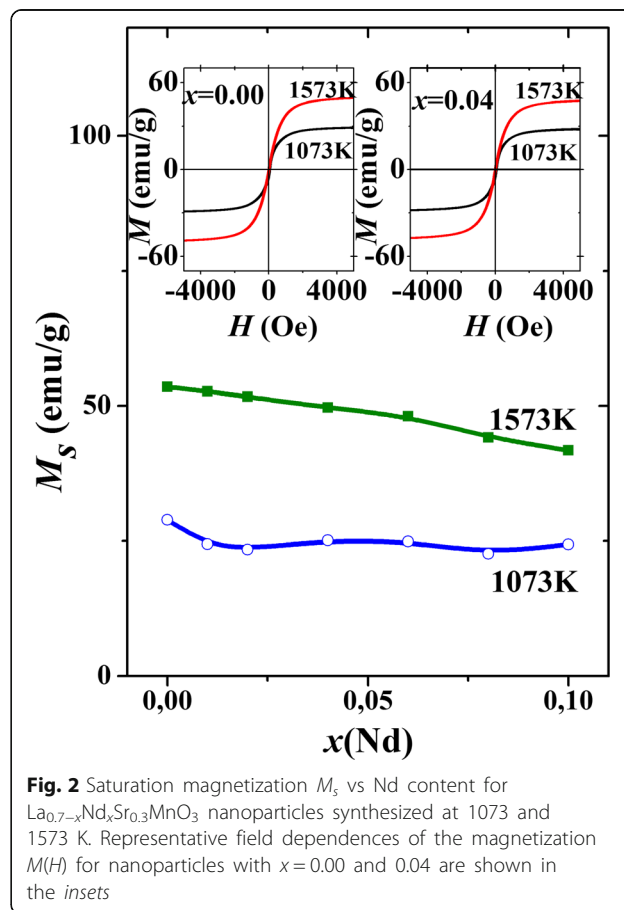
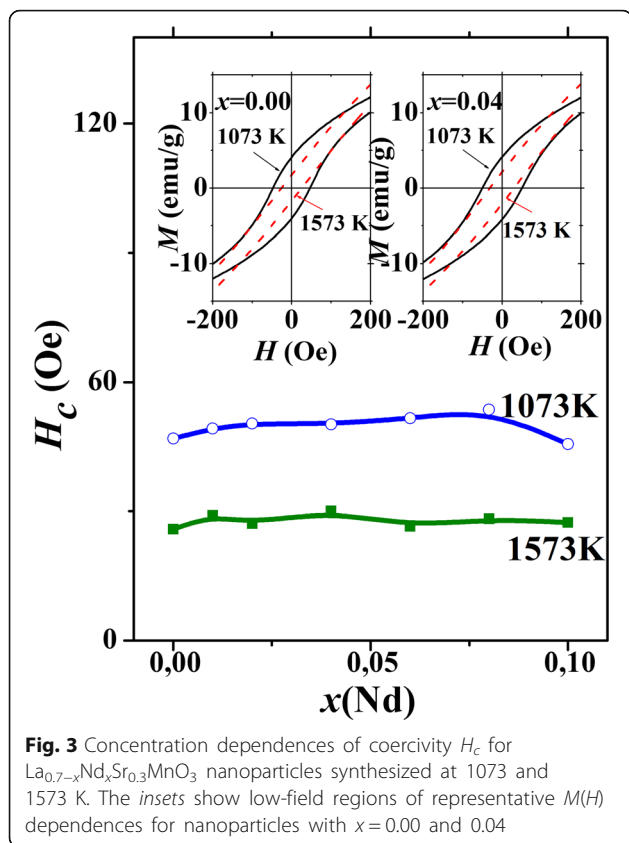


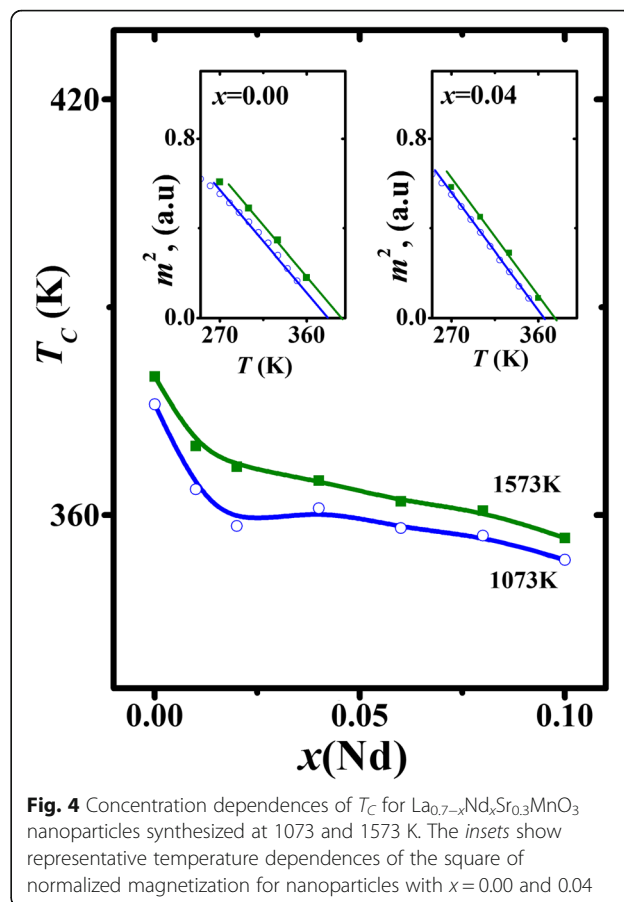
Fig. 2 Saturation magnetization M_s vs Nd content for $\text{La}_{0.7-x}\text{Nd}_x\text{Sr}_{0.3}\text{MnO}_3$ nanoparticles synthesized at 1073 and 1573 K. Representative field dependences of the magnetization $M(H)$ for nanoparticles with $x = 0.00$ and 0.04 are shown in the insets



series of samples, is likely to originate from the enhanced inhomogeneity of these samples.

Magnetic state of nanoparticles is usually quite inhomogeneous due to significant contribution from the surface layer, whose properties differ from the properties of the nanoparticle core, and due to the scatter in particle size. It is shown in [36, 37] that the temperature behavior of particle ensembles can be satisfactory as described by the average Curie temperature concept. In this case, it is expected that the behavior of the ensembles' magnetization will obey the law $M(T) \sim \sqrt{T_C - T}$.

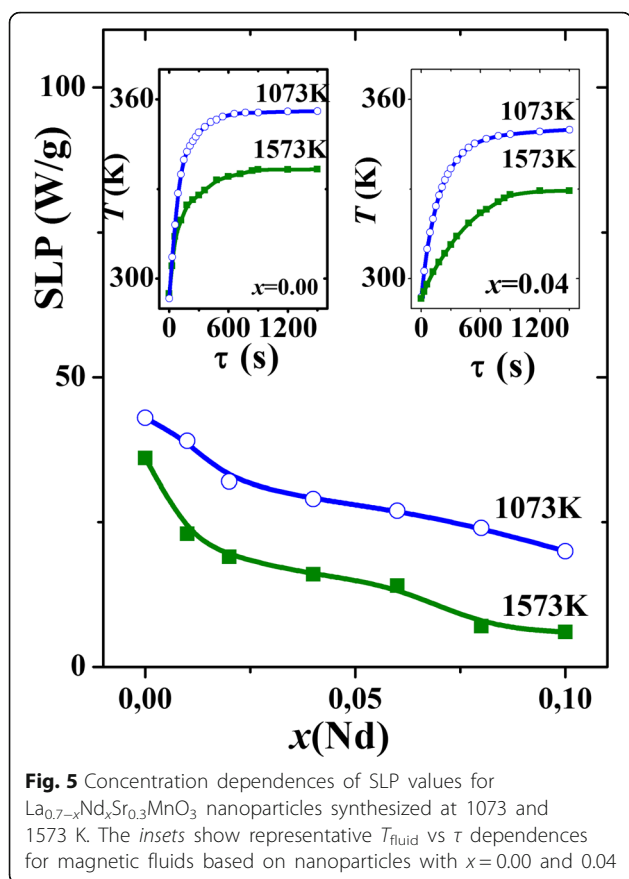
The insets to Fig. 4 show the representative temperature dependences of the square of normalized magnetization $m = M(T, H = 5 \text{ kOe})/M(110 \text{ K}, H = 5 \text{ kOe})$ for $\text{La}_{0.7-x}\text{Nd}_x\text{Sr}_{0.3}\text{MnO}_3$ nanoparticles synthesized at 1573 and 1073 K. It is seen that there is a wide temperature range where such dependences are linear (see straight solid lines in the insets to Fig. 4). The Curie temperature values can be estimated from these dependences by the points of intersection of linear area with the temperature axis. Concentration dependences of $T_C(x)$ for both series of samples are shown in Fig. 4. In both cases, T_C decreases with growing Nd content. At the same time, all samples synthesized at lower temperature have lower Curie point.



To characterize the heating efficiency of the nanoparticles, magnetic fluids based on them and aqueous agarose solution were prepared and subjected to AC magnetic field. Dependence of the temperature of magnetic fluid (T_{fluid}) vs time resided in AC field (τ) with fixed amplitude H_{max} , and frequency f makes it possible to calculate SLP values.

Representative $T_{\text{fluid}}(\tau)$ dependences for magnetic fluids based on $\text{La}_{0.7-x}\text{Nd}_x\text{Sr}_{0.3}\text{MnO}_3$ nanoparticles with $x=0.00$ and 0.04 are shown in the insets to Fig. 5. The measurements were performed in magnetic field with amplitude $H_{\text{max}} = 9.3 \text{ kA/m}$ and frequency $f = 300 \text{ kHz}$. It can be seen that all samples effectively heat up under the action of AC magnetic field. However, the heating efficiency of manganites decreases with growing the Nd content.

Figure 5 shows the SLP values calculated according to formula (2). It should be mentioned that the application of these nanoparticles allows one to provide heating to certain constant temperature (saturation temperature T_S). An interesting feature is that SLP values for nanoparticles synthesized at higher temperature are lower, than corresponding values for those synthesized at lower temperature. The insets to Fig. 3 may provide the



explanation for this fact: the coercivity of the samples synthesized at 1073 K exceeds H_c for the samples obtained at 1573 K. At the same time, the magnetization in the weak-field range does not strongly differ for both kinds of samples. As a result, the area of the hysteresis loop in the first case is greater than in the second case. Since SLP is proportional to the area of hysteresis loop [37], its values are greater in the samples synthesized at 1073 K.

It is seen from the insets to Fig. 5 that after sharp initial rise, the change of T_{fluid} with τ becomes slower and eventually T_{fluid} goes to saturation. The saturation

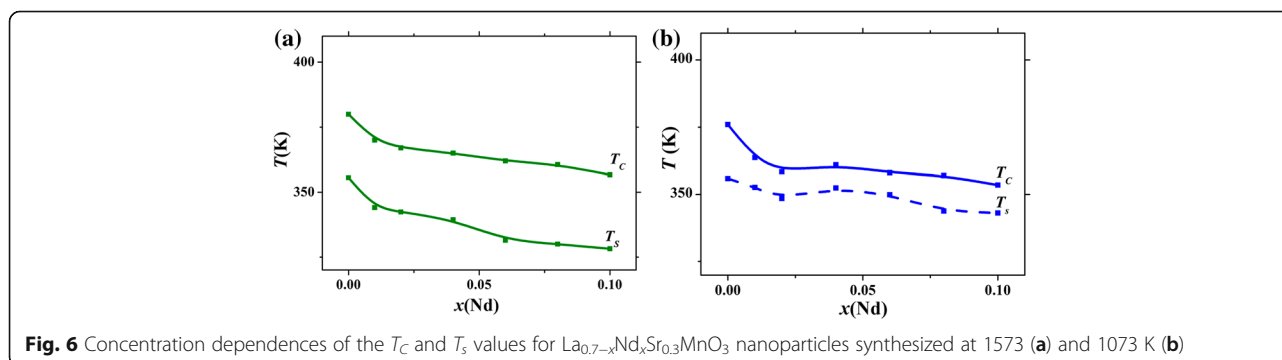
temperature T_s decreases with the increase in the Nd content. Figure 6 compares the T_C and T_s values for $\text{La}_{0.7-x}\text{Nd}_x\text{Sr}_{0.3}\text{MnO}_3$ nanoparticles synthesized at different temperatures. It is seen that the character of T_C vs x dependences is close to that of T_s vs x ones. At the same time, the values of T_s , although being close to T_C , never exceed the T_C values. This implies that heat transfer to the surrounding environment may play an important role, and such effect should be taken into account when using the magnetic fluids under real conditions.

Based on the results of complex investigations, one can conclude that the modification of $\text{La}_{1-y}\text{Sr}_y\text{MnO}_3$ manganite nanoparticles, particularly by partial substitution of La by Nd, strongly affects their properties. At the same time, crystallographic and magnetic parameters may display non-monotonous dependence on Nd content, and this phenomenon may become more pronounced in the samples synthesized at lower temperatures.

Conclusions

The effect of synthesis temperature on the structural and magnetic properties of $\text{La}_{0.7-x}\text{Nd}_x\text{Sr}_{0.3}\text{MnO}_3$ ($x=0.00-0.1$) nanoparticles was investigated in this study. It was shown that for nanoparticles synthesized at 1573 K, both crystallographic and magnetic parameters monotonously change with changing Nd content. The obtained result are in good agreement with literature data for bulk counterparts and can be explained by the enhancement of the local distortions of crystal lattice upon partial substitution of La^{3+} ions by Nd^{3+} ones.

For the samples synthesized at 1073 K, both crystallographic and magnetic parameters display non-monotonous dependence on Nd content. This fact can be explained either by incomplete ordering of the crystal structure or by the dependence of the degree of oxygen non-stoichiometry on chemical composition (in this case—on Nd content). Since magnetic nanoparticles are mainly synthesized at relatively low temperatures, such features have to be taken into account in researching and predicting the particles' properties.



Funding

The work is partially supported by the Program on Fundamental Studies of the National Academy of Science of Ukraine "FineChemicals" No7/16, by the Project from the Department of Targeted Training of Taras Shevchenko National University of Kyiv at the NAS of Ukraine, and by the Joint Ukraine-India research project.

Authors' Contributions

YuS and SS synthesized the corresponding nanoparticles, designed and performed the X-ray experiments and heating efficiency study, and analyzed the obtained data. AB, MK, and VK performed the investigations of field dependences of magnetization and analyzed the obtained data. YuTP and AT performed the investigations of temperature dependences of magnetization and analyzed the obtained results. YuS and AT contributed in the drafting and revision of the manuscript. AG supervised the work and finalized the manuscript. All authors read and approved the final manuscript.

Competing Interests

The authors declare that they have no competing interests.

Author details

¹V.I. Vernadskii Institute of General and Inorganic Chemistry of the NAS of Ukraine, 32/34 Palladina Ave., Kyiv 03142, Ukraine. ²Institute of Physics of the NAS of Ukraine, 46 Nauky Ave., Kyiv 03028, Ukraine. ³Institute of Magnetism of the NAS of Ukraine and MES of Ukraine, 36-b Vernadsky Blvd., Kyiv 03680, Ukraine.

Received: 26 December 2016 Accepted: 31 January 2017

Published online: 08 February 2017

References

- Weissleder R, Elizondo G, Wittenburg J, Rabito CA, Bengel HH, Josephson L (1990) Ultrasmall superparamagnetic iron oxide: characterization of a new class of contrast agents for MR imaging. *Radiology* 175:489–493
- Yadollahpour A, Rashidi S (2015) Magnetic nanoparticles: a review of chemical and physical characteristics important in medical applications. *Orient J Chem* 31:271–277
- Salata OV (2004) Applications of nanoparticles in biology and medicine. *J Nanobiotechnol* 2:3
- Belous AG, Solopan SO, Yelenich OV, Tovstolytkin AI, Kolodiaznyh TV, Osinsky SP, Bubnovskaya LN (2014) Nanoparticles of spinel and perovskite ferromagnets and prospects for their application in medicine. *AIP Conf Proc* 1627:13–18
- Xu C, Mu L, Roes I, Miranda-Nieves D, Nahrendorf M, Ankrum JA, Zhao W, Karp JM (2011) Nanoparticle-based monitoring of cell therapy. *Nanotechnol* 22:494001
- Panatarotto D, Prtidos CD, Hoebeke J, Brown F, Kramer E, Briand JP, Muller S, Prato M, Bianco A (2003) Immunization with peptide-functionalized carbon nanotubes enhances virus-specific neutralizing antibody responses. *Chem&Biol* 10:961–966
- Wang Y-XJ (2011) Superparamagnetic iron oxide based MRI contrast agents: current status of clinical application. *Quant Imaging Med Surg* 1:35–40
- Pérido EA, Hemery G, Sandre O, Ortega D, Garaio E, Plazaola F, Teran FJ (2015) Fundamentals and advances in magnetic hyperthermia. *Appl Phys Rev* 2:041302
- Sousa ME, Carrea A, Zélis PM, Muraca D, Mykhaylyk O, Sosa YE, Goya RG, Sánchez FH, Dewey RA, Fernández van Raap MB (2016) Stress-induced gene expression sensing intracellular heating triggered by magnetic hyperthermia. *J Phys Chem C* 120:7339–7348
- Wang Y, Xu C, Ow H (2013) Commercial nanoparticles for stem cell labeling and tracking. *Theranostics* 3:544–560
- Cromer Berman SM, Walczak P, Bulte JWM (2011) Tracking stem cells using magnetic nanoparticles. *WIREs Nanomed Nanobiotechnol* 3:343–355
- Loai Y, Ganesh T, Cheng H-LM (2012) Concurrent dual contrast for cellular magnetic resonance imaging using gadolinium oxide and iron oxide nanoparticles. *Int J Mol Imag*. 2012: Article ID 230942.
- Lee N, Hyeon T (2012) Designed synthesis of uniformly sized iron oxide nanoparticles for efficient magnetic resonance imaging contrast agents. *Chem Soc Rev* 41:2575–2589
- Wang F, Tan WB, Zhang Y, Fan X, Wang M (2006) Luminescent nanomaterials for biological labelling. *Nanotechnol* 17:R1–R13
- Laurent S, Dutz S, Hafeli UO, Mahmoudi M (2011) Magnetic fluid hyperthermia: focus on superparamagnetic iron oxide nanoparticles. *Adv Coll Interf Sci* 166:8–23
- Dutz S, Hergt R (2014) Magnetic particle hyperthermia—a promising tumour therapy? *Nanotechnol* 25:452001
- Pradhan AK, Bah R, Konda RB, Mundle R, Mustafa H, Bamiduro O, Rakhimov RR, Wei X, Shellmyer J (2008) Synthesis and magnetic characterizations of manganite-based composite nanoparticles for biomedical applications. *J Appl Phys* 103:07F704
- Nikiforov VN, Koksharov YA, Polyakov SN, Malakho AP, Volkov AV, Moskvina MA, Khomutov GB, Irkhin VY (2013) Magnetism and Verwey transition in magnetite nanoparticles in thin polymer film. *J Alloy Compd* 569:58–61
- Dagotto E, Hotta T, Moreo A (2001) Colossal magnetoresistant materials: the key role of phase separation. *Phys Rep* 344:1–153
- Loktev VM, Pogorelov YG (2000) Peculiar physical properties and the colossal magnetoresistance of manganites (Review). *Low Temp Phys* 26:171–192
- Gaudon M, Laberty-Robert C, Ansart F, Stevens P, Rousset A (2002) Preparation and characterization of $\text{La}_{1-x}\text{Sr}_x\text{MnO}_{3+6}$ ($0 \leq x \leq 0.6$) powder by sol-gel processing. *Solid State Sci* 4:125–133
- Shlapa Y, Kulyk M, Kalita V, Polek T, Tovstolytkin A, Grenèche J-M, Solopan S, Belous A (2016) Iron-doped (La, Sr)MnO₃ manganites as promising mediators of self-controlled magnetic nanohyperthermia. *Nanoscale Res Lett* 11:24
- Singh D, Mahajan A (2015) Effect of A-site cation size on the structural, magnetic, and electrical properties of $\text{La}_{1-x}\text{Nd}_x\text{Mn}_{0.5}\text{Cr}_{0.5}\text{O}_3$ perovskites. *J All Compd* 25:172–179
- Kjær J, Krogh Andersen IG, Skou E (1998) Thermogravimetric studies of oxygen stoichiometry and oxygen transport kinetics in lanthanum strontium ferrite manganites. *Solid State Ionics* 113–115:387–392
- Kharton VV, Kovalevsky AV, Patrakeev MV, Tsipis EV, Viskup AP, Kolotygin VA, Yaremchenko AA, Shaula AL, Kiselev EA, Waerenborgh JC (2008) Oxygen nonstoichiometry, mixed conductivity, and Mossbauer spectra of $\text{Ln}_{0.5}\text{A}_{0.5}\text{FeO}_{3-\delta}$ (Ln = La – Sm, A = Sr, Ba): effects of cation size. *Chem Mater* 20:6457–6467
- Atsumi T, Ohgushi T, Namikata H, Kamegashira N (1997) Oxygen nonstoichiometry of $\text{LnMnO}_{3-\delta}$ (Ln = La, Pr, Nd, Sm and Y). *J All Compd* 252:67–70
- Zvatora P, Veverka M, Veverka P, Knizek K, Zaveta K, Polleert E, Kral V, Goglio G, Duguet E, Kaman O (2013) Influence of surface and finite size effects on the structural and magnetic properties of nanocrystalline lanthanum strontium perovskite manganites. *J Solid State Chem* 204:373–379
- Grossin D, Noudem JG (2004) Synthesis of fine $\text{La}_{0.8}\text{Sr}_{0.2}\text{MnO}_3$ powder by different ways. *Solid State Sci* 6:939–944
- Belous AG, Vyunov OI, Pashkova EV, Yanchevskii OZ, Tovstolytkin AI, Pogorily AN (2003) Effects of chemical composition and sintering temperature on the structure of $\text{La}_{1-x}\text{Sr}_x\text{MnO}_{3 \pm y}$ solid solutions. *Inorg Mater* 39:161–170
- Bubnovskaya L, Belous A, Solopan S, Kovelskaya A, Bovkun L, Podoltsev A, Kondratenko I, Osinsky S (2014) Magnetic fluid hyperthermia of rodent tumors using manganese perovskite nanoparticles. *J Nanopart* 2014:278761
- Vasseur S, Duguet E, Portier J, Goglio G, Mornet S, Hadova E, Knizek K, Marysko M, Veverka P, Pollert E (2006) Lanthanum manganese perovskite nanoparticles as possible in vivo mediators for magnetic hyperthermia. *J Magn Magn Mater* 302:315–320
- Solopan S, Belous A, Yelenich A, Bubnovskaya L, Kovelskaya A, Podoltsev A, Kondratenko I, Osinsky S (2011) Nanohyperthermia of malignant tumors. I. Lanthanum-strontium manganite magnetic fluid as potential inducer of tumor hyperthermia. *Exp Oncol* 33:30–135
- Monshi A, Foroughi MR, Monshi MR (2012) Modified Sherrer equation to estimate more accurately nanocrystallite size using XRD. *World J Nanosci Nanotechnol* 2:1062–1071
- Veverka M, Zaveta K, Kaman O, Veverka P, Knizek K, Pollert E, Burian M, Kaspar P (2014) Magnetic heating by silica-coated Co–Zn ferrite particles. *J Phys D Appl Phys* 47:065503–065511
- Maguire ET, Coats AM, Shakle JMS, West AR (1999) Stoichiometry and defect structure of 'NdMnO₃'. *J Mater Chem* 9:1337–1346
- Kalita VM, Tovstolytkin AI, Ryabchenko SM, Yelenich OV, Solopan SO, Belous AG (2015) Mechanisms of AC losses in magnetic fluids based on substituted manganites. *Phys Chem Chem Phys* 17:18087–18097
- Kalita VM, Lozenko AF, Ryabchenko SM, Timopheev AA, Trotsenko RA, Danilenko IA, Konstantinova TE (2008) Magnetic properties of $\text{La}_{0.7}\text{Sr}_{0.3}\text{MnO}_3$ nanopowders. *Low Temp Phys* 34:436–445